Controlled oxygen vacancies and space correlation with Cr^{3+} in $SrTiO_3$

F. La Mattina,[1,2,3] J. G. Bednorz,[2] S. F. Alvarado,[2] A. Shengelaya,[4] K. A. Müller,[1] and H. Keller[1]
[1]*Physik-Institut der Universität Zürich, Winterthurerstr. 190, CH-8057 Zürich, Switzerland*
[2]*IBM Research, Zurich Research Laboratory, Säumerstr. 4, CH-8803 Rüschlikon, Switzerland*
[3]*EMPA, Swiss Federal Laboratories for Materials Testing and Research, Electronics/Metrology Laboratory, 8600 Dübendorf, Switzerland*
[4]*Physics Institute of Tbilisi State University, Chavchavadze 3, GE-0128 Tbilisi, Georgia*
(Received 4 June 2009; revised manuscript received 13 July 2009; published 31 August 2009)

By means of electron paramagnetic resonance (EPR) measurements on thermally reduced Cr-doped $SrTiO_3$, we find a strong correlation between the Cr^{3+} ions and oxygen vacancies (V_os). A charge compensation associated with the creation of V_os induced by thermal reduction causes the valence of the Cr ions to change from 4+ to 3+. This induces a symmetry change in the crystal field experienced by the Cr atom from cubic to axial. On the other hand, in Cr/Nb-codoped samples, where V_os are absent, the Cr^{3+} EPR signal is isotropic, indicating that these Cr ions occupy an octahedral site of cubic symmetry. From the angular dependence of the EPR spectra we determine an axial crystal field parameter ($D \simeq 8$ MHz), which is consistent with a perturbation induced by a V_o localized at the third coordination sphere of Cr^{3+}. This is in contrast to other transition-metal dopants, where the V_o is located at the first coordination sphere. Thus we identify a linear complex of the form Cr^{3+}-O-Ti^{3+}-V_o-Ti^{3+}, which is unique in its structure, and which, furthermore, might account for the stabilization of the insulating state in reduced Cr-doped $SrTiO_3$ crystals.

DOI: 10.1103/PhysRevB.80.075122 PACS number(s): 71.27.+a, 71.55.−i, 72.15.Rn, 71.30.+h

I. INTRODUCTION

The electrical transport properties of perovskite oxides can be controlled by inducing a deliberate deviation from the ideal stoichiometry.[1] The introduction of mobile charge carriers through the control of ionizable impurities is central to the production of semiconductor devices. In $SrTiO_3$ an insulator-to-metal transition is obtained at a small critical density of electron doping of $\sim 10^{18}$ e/cm^3.[2] Moreover, various cations confer substantial modifications of the electronic properties. For instance, pure reduced, and Nb-doped $SrTiO_3$ have been reported to exhibit single-gap[3,4] and two-gap superconductivity,[5] respectively. The capability of controlling point defects, such as oxygen vacancies (V_os) or transition-metal (TM) dopants, is essential for the development of semiconducting electronic devices based on perovskite compounds.[6–9] Current-induced bistable resistance effects on metal-insulator-metal (MIM) structures based on doped perovskite oxides, such as Cr-doped $SrTiO_3$, have attracted substantial interest because of their potential technological applications for nonvolatile memory devices.[10,11] Although various models have been proposed for the resistive switching in $SrTiO_3$,[12–14] a clear understanding of the role and the nature of intrinsic defects or dopants has not yet been achieved. Extended defects, such as dislocations[15] and local changes of the V_o content,[13,16–18] are proposed to be responsible for electron conduction in $SrTiO_3$. The accumulation of V_os in a confined conductive path (filamentary) has experimentally been shown[12,13] to result from a dc electroconditioning procedure.[7,9] Local reduction/oxidation processes have been proposed by some authors as an explanation for the resistance-switching mechanism,[17,19] in contradiction to other experimental evidence of trapping/detrapping processes involving the Cr dopant.[8,9] A promising concept for tailoring electronic properties on the nanometer scale arises from the possibility of creating V_os in confined regions.[17,18,20,21] The formation of V_o is accompanied by the transfer of two electrons to the 3d(z^2) orbitals of the two Ti atoms along the Ti-V_o-Ti axis[22] and, at higher content of V_o, an insulator-to-metal transition occurs.[23,24] Moreover, it has been proposed that the spatial distribution of the Ti^{3+}-V_o-Ti^{3+} complex[18,25,26] can induce an enhancement or a decrease in the carrier density.

In this paper, we present a detailed electron paramagnetic resonance (EPR) study of thermally reduced Cr-doped $SrTiO_3$. Based on this EPR analysis, we extract a model that describes the spatial correlation between the V_os and the Cr ions in the bulk and explains how this correlation accounts for the transport properties of $SrTiO_3$.

II. MATERIALS AND METHODS

Nominally pure $SrTiO_3$ and Cr-doped and Cr/Nb-codoped crystals were grown from stoichiometric ceramic by the floating-zone method in synthetic air (N_2/O_2).[27] The starting material was prepared by solid-state reaction of a stoichiometric mixture of $SrCO_3$ and TiO_2 at 1150 °C. The $SrCO_3$ has a purity level of 99.999%, whereas the TiO_2 has Fe and Cr at levels of 40 and 1 ppm, respectively. Cr_2O_3 or $SrCrO_4$ were admixed to $SrTiO_3$ to obtain Cr-doping levels in the range of 0.001 to 0.2 mol % or 0.4 to 2 mol %, respectively. The crystals obtained have a cylindrical shape, with a typical diameter and length of ~4 mm and ~4 cm, respectively. Two series of crystals were annealed for 6 h at 1150 °C either in O_2 or Ar/H_2 (5%). The samples were cut along the ⟨100⟩ crystallographic axis with typical dimensions of $2 \times 1 \times 0.2$ mm^3, and polished for the EPR and optical absorption (OA) measurements. EPR spectra were taken with a Bruker EMX™ system at 9.4 GHz (*X* band). A manually operated Bruker ER 218G1 goniometer was used to rotate the sample inside the EPR cavity to study the angular dependence of the EPR signal with respect to the external field.

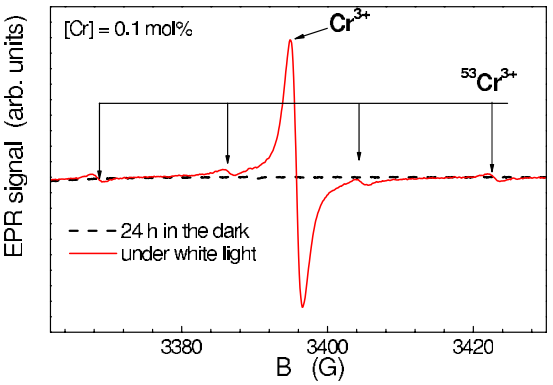

FIG. 1. (Color online) Photoinduced Cr^{3+} EPR signal in oxidized $SrTiO_3$:Cr 0.1 mol %. Solid red line: Cr^{3+} EPR signal detected under illumination with white light. The signal decays when the light is switched off, and disappears completely after 24 h (dashed black line).

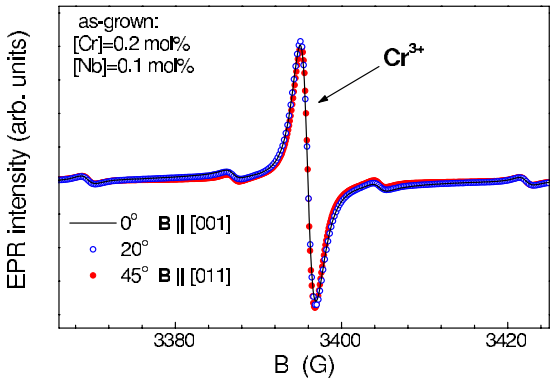

FIG. 2. (Color online) Cr^{3+} EPR signal in Cr/Nb-codoped as-grown $SrTiO_3$. The spectra are obtained by rotating the sample around the [100] crystal axis. The signals at all angles overlap, indicating a cubic site symmetry (isotropic EPR signal).

OA spectra in the near-infrared, visible, and UV range were taken at room temperature with a Beckman DU® 650 spectrometer.

III. EXPERIMENT AND RESULTS

A. Cr^{3+} site symmetry

In $SrTiO_3$, the Cr dopant substitutes Ti^{4+}, and in case of perfect oxygen stoichiometry occupies the octahedral site in the 4+ valence state. The trivalent state can be produced under illumination with a photon energy above 1.5 eV owing to a charge-transfer excitation from the valence band to the Cr 3*d* orbitals.[28] At room-temperature excitation with a photon energy above ca. 3.2 eV creates a conduction-band (CB) electron via an indirect band-gap transition,[29,30] which generates Cr^{3+} via a subsequent trapping process. In both cases, the 3+ state is unstable, and all Cr centers relax back to the 4+ valence state when the light is switched off.[28,31,32]

Cr^{4+} has spin $S=1$, and is EPR silent at the *X* band owing to a strong crystal-field splitting.[33] A direct detection of Cr^{4+} requires measurements at higher frequencies (*Q* band).[33,34] Figure 1 shows an EPR spectrum of photon generated (white light) Cr^{3+} in a stoichiometric sample and the spectrum recorded after storing the sample in the dark for 24 h. The spectrum under illumination consists of a central line ($g \approx 1.978$) resulting from the 3+ state of the ^{50}Cr, ^{52}Cr, and ^{54}Cr isotopes and a hyperfine quartet resulting from the nuclear-spin coupling ($I_n=\frac{3}{2}$) of the ^{53}Cr isotope (natural abundance 9.5%).[35]

We measured this EPR signal in a series of Cr-doped oxidized crystals, from nominally pure (0.0001 mol %) to 2 mol %, and could observe the Cr^{3+} signal only under light exposure. This suggests that in our crystals only the 4+ valence state is possible, unless an electron donor is present. However, several examples of stable Cr^{3+} have been reported in the literature.[35–38] For instance, in oxidized Cr-doped $SrTiO_3$ grown by the flame fusion method (Verneuil) a clear example has been observed by Meilerling.[37] By means of EPR he found two kinds of Cr^{3+} centers: a main EPR signal from cubic octahedral Cr^{3+} ions, and only a 4000 times weaker signal from orthorhombic Cr^{3+} centers with charge compensation involving oxygen vacancies. The difference with respect to our oxidized samples may originate from the technique used for the crystal growth. Thus, one can see that the charge state and symmetry of Cr ions in $SrTiO_3$ strongly depend on the quality of the crystal and its impurity concentrations. In our case, the floating-zone technique used for the crystal growth allows to reduce the dislocations density by up to three orders of magnitude as compared to the Verneuil method ($10^2 \sim 10^3/cm^2$ for floating-zone[39] and $\sim 10^6/cm^2$ for Verneuil).[40]

To characterize the Cr^{3+} symmetry in a stable state, we used a crystal with Cr/Nb co-doping, where Nb acts as electron donor. A Cr amount of twice the Nb content ([Cr] =0.2 mol%, [Nb]=0.1 mol%) was chosen to ensure a total compensation of the electron donors, which preserves the insulating state, a prerequisite for unambiguous EPR measurements. EPR signals recorded at different angles between the crystallographic axes and the magnetic field $\vec{\mathbf{B}}$ are shown in Fig. 2, where [100] is the rotation axis and $\theta=0$ for $\vec{\mathbf{B}} \| [001]$. The EPR spectra recorded at different angles overlap. This isotropy indicates that Cr^{3+} occupies a site of cubic symmetry. In the case of Cr-doped samples annealed in Ar/H_2 atmosphere, however, a perturbation of the Cr^{3+} site symmetry is apparent. This is shown in Fig. 3, which compares the EPR signal of the Cr/Nb-codoped sample with the Cr-doped reduced sample. In the latter the Cr content is lower, therefore the broadening of the EPR signal cannot be explained in terms of magnetic dipolar interaction. Thus the EPR lineshape change must originate from a site-symmetry modification (noncubic). This is explicitly demonstrated by the angular dependence of the EPR spectra for all Cr concentrations. In particular, at a doping ≤ 0.01 mol%, the narrow width ($\simeq 1.4$ G peak-to-peak) of the EPR lines allows the identification of an additional broad anisotropic line overlapping with the Cr^{3+} line. Here one can clearly separate the hyperfine line at ~ 3422 G (Fig. 4(c)) from the central line of Cr^{3+} at ~ 3400 G (Fig. 4(b)). Both lines exhibit the same changes under a rotation of the crystal by $\frac{\pi}{2}$ around the [100]

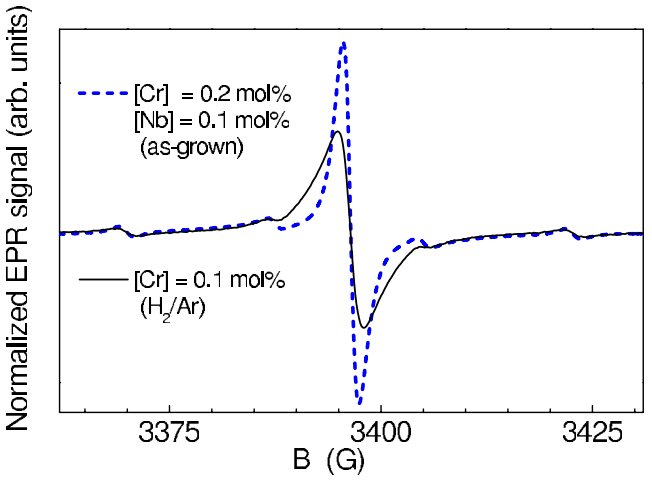

FIG. 3. (Color online) Comparison of Cr^{3+} EPR signals in $SrTiO_3$ with different site symmetries. Dashed blue line: isotropic signal detected in as-grown Cr/Nb-codoped sample; solid black line: signal detected in an oxygen-reduced Cr-doped sample. The spectra are normalized to the total number of spins (double integral of EPR signal).

axis. As the four satellite lines are a fingerprint of $^{53}Cr^{3+}$, the anisotropic component must be assigned to a Cr spin center.

B. Cr^{3+}-oxygen vacancy complex

The Cr^{3+} EPR signal observed in the crystal annealed in Ar/H_2 points to the creation of V_os as electron donors.

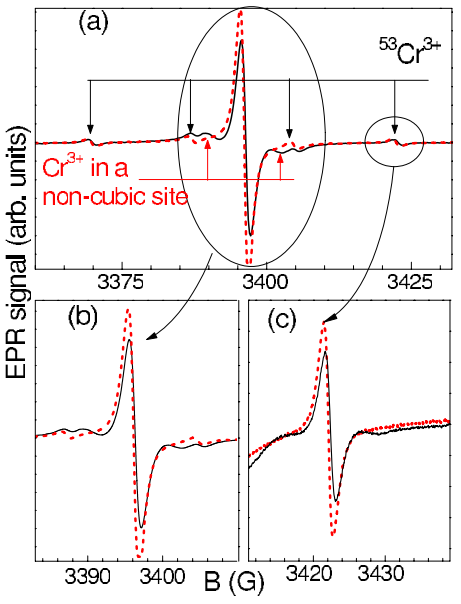

FIG. 4. (Color online) EPR spectra of oxygen-reduced Cr-doped $SrTiO_3$:Cr0.01 mol%). (a) Solid black line: *B* parallel to the [001] crystal axis; dashed red line: *B* parallel to the [011] axis. The narrow linewidth at this Cr content allows a precise comparison of the lineshape of the central line (b) of Cr^{3+} with the hyperfine line (c) of ^{53}Cr at ~3422 G ($I_n=\frac{3}{2}$). The identical changes on both lines indicate that the anisotropic component can only originate from a Cr spin center.

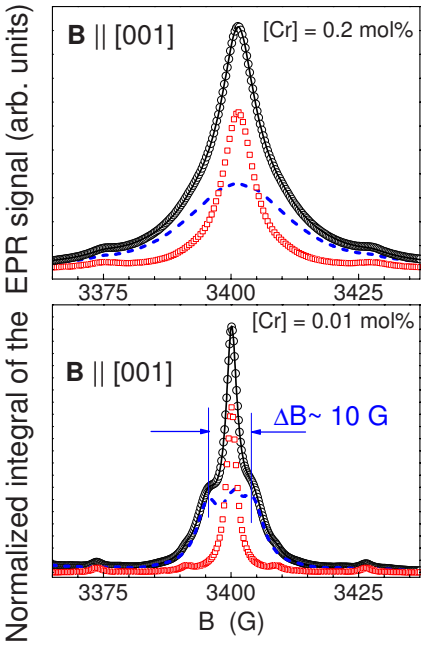

FIG. 5. (Color online) Integral of the EPR signal of reduced Cr-doped $SrTiO_3$ for two different Cr concentrations. Black circles: measured spectrum; solid black line: fitted spectrum; open red squares: the isotropic line; dashed blue line: the anisotropic component obtained as the difference between the measured data and the fitted red component.

Therefore the anisotropic component of the EPR signal should be related to a local lattice distortion due to the proximity of a V_o. A narrow isotropic and a broad anisotropic component can be clearly separated in the EPR spectra, independently of the Cr-doping level. Figure 5 shows the deconvolution performed for two different representative Cr concentrations, 0.01 and 0.2 mol %. The integrated EPR spectra were deconvoluted into a narrow and a broad component, both consisting of a central line and four hyperfine lines. All lines are well described by a Lorentzian lineshape. The shape and the position of the narrow component were found to be identical for each angle and can easily be separated from the broad anisotropic component. The dashed lines in Fig. 5 represent the anisotropic components, obtained as difference between the experimental data and the fitted isotropic components. The relative weights of the isotropic and the anisotropic contributions were found to be ~40% and ~60%, respectively. This ratio is constant for all Cr concentrations analyzed (0.001 to 2 mol %).

This fact indicates that both the charge compensation mechanism and the origin of the noncubic Cr site are identical for all samples and involve the full amount of Cr. However, for the analysis of the angular dependence of the EPR lines, the sample with the lower Cr content is not adequate because of the presence of Fe impurity, which interferes with the fitting procedure. Therefore a sample with a Cr content of 0.2 mol % was chosen. Moreover, the dimensions of the sample were chosen to be $0.5\times0.5\times0.5$ mm^3 to avoid possible contributions caused by shape anisotropies due to different mechanical stress. In Fig. 6, the angular dependence of the anisotropic component of the EPR spectra is shown. The

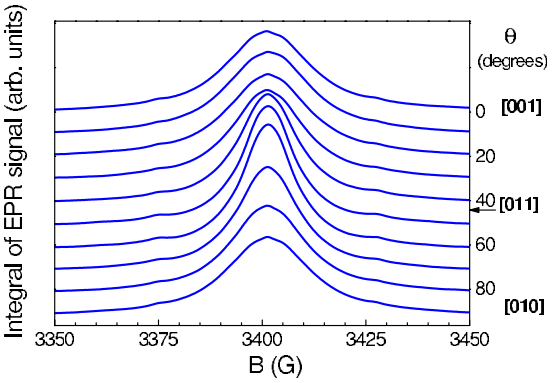

FIG. 6. (Color online) Angular dependence of the anisotropic component of the EPR signal for the Cr-doped (0.2 mol %) reduced sample. Sample rotation is around the [100] crystal axis. The [001] and the [010] axes are indistinguishable for a cubic crystal.

broad component of the spectrum reported in Fig. 5 (dashed line) indicates the presence of at least three lines within a range of 5 G from the center. This small shift suggests an analysis of the EPR spectra in terms of an effective spin Hamiltonian for Cr^{3+} in the limit of a weak crystal field. We tentatively use an axial symmetric crystal-field term in the spin Hamiltonian:[41]

$$\mathcal{H} = \beta \vec{\mathbf{B}} \cdot \tilde{\mathbf{g}} \cdot \vec{\mathbf{S}} + hD\left(S_z^2 - \frac{1}{3}S \cdot (S+1)\right). \tag{1}$$

Here β is the Bohr magneton, $\vec{\mathbf{B}}$ is the magnetic field, the $\tilde{\mathbf{g}}$ tensor is assumed to be isotropic ($g \approx 1.978$), $\vec{\mathbf{S}}$ is the spin vector (S_x, S_y, S_z), h is Planck's constant, D is the crystal-field operator describing the axial symmetry (here measured in GHz), and $S=\frac{3}{2}$. The weak crystal-field condition is obtained by the limiting condition of $D \ll \sim 9.4$ GHz (the microwave energy used). Under this condition, it is possible to solve the effective Hamiltonian with a perturbation approach and obtain the following resonant magnetic fields (B_{res}) for the three allowed transitions:[42,43]

$$\left(-\frac{1}{2} \leftrightarrow +\frac{1}{2}\right): B_{\mathrm{res}} = B_0 \tag{2}$$

$$\left(-\frac{3}{2} \leftrightarrow -\frac{1}{2}\right): B_{\mathrm{res}} = B_0 + \Delta B_0(3\cos\theta^2 - 1) \tag{3}$$

$$\left(+\frac{1}{2} \leftrightarrow +\frac{3}{2}\right): B_{\mathrm{res}} = B_0 - \Delta B_0(3\cos\theta^2 - 1). \tag{4}$$

Here $\Delta B_0 = \frac{hD}{g\beta}$ Eq. (2) describes an isotropic line corresponding to the transition $-\frac{1}{2} \leftrightarrow +\frac{1}{2}$, and Eqs. (3) and (4) describe two anisotropic lines that are symmetrically spaced around the central line. The relative amplitudes of the three spectral contributions are 3:4:3,[41] yielding a fraction of $\frac{4}{4+6}$ (40%) for the isotropic and $\frac{6}{4+6}$ (60%) for the anisotropic contribution, in excellent agreement with our experiments. As this intensity ratio was found to be independent of the Cr doping level (as mentioned earlier), we can conclude that each Cr occupies a site of axial symmetry. Therefore, a space correlation

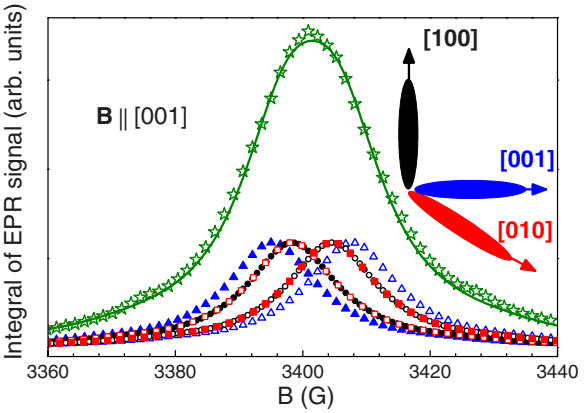

FIG. 7. (Color online) Anisotropic component of the Cr^{3+} integrated EPR signal in the reduced Cr-doped sample ([Cr] =0.2 mol%). The spectra were fitted by six Lorentzians (two for each crystal axis) using only two free parameters: the crystal-field parameter D and the linewidth w. The positions of the lines were obtained from Eqs. (3) and (4) adapted for each direction. Blue triangles, filled and open: lines relative to the [001] crystal axis; red squares, filled and open: lines relative to [010] axis; black circles, filled and open: lines of the [100] axis; green stars: the anisotropic component extracted from the experimental data; green line: sum of all fitted lines.

between the Cr^{3+} and the V_o is present, and is responsible for the site symmetry. To estimate the axial crystal-field parameter D defined in Eq. (1), a fitting model for the anisotropic spectral component was implemented by using Eqs. (3) and (4). In Fig. 7, a multiple line fit is shown for $\theta=0$, where six Lorentzian lines (two each for the [001], [010], and [100] crystal axes) were used. Equations (3) and (4) describe the contribution of the [001] crystal axis, whereas the [010] contribution can be obtained by replacing θ with $\frac{\pi}{2}-\theta$. The [100] rotation axis gives rise to two constant components for $\theta=\frac{\pi}{2}$. Assuming that all lines have the same linewidth w, the spectra in Fig. 6 were analyzed using only two free param-

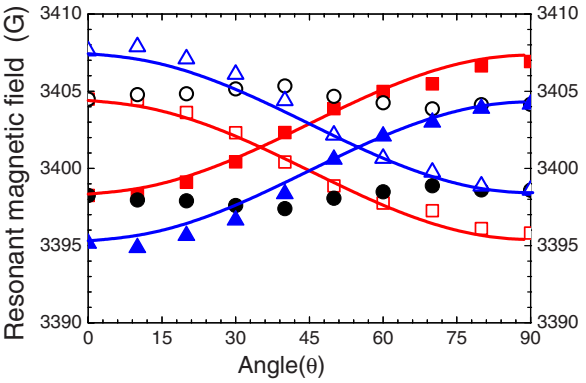

FIG. 8. (Color online) Angular dependencies of the EPR transitions of Cr^{3+} in $SrTiO_3$ in an axial crystal field. The symbols describe the peak position of the transitions shown in Fig. 7. The solid lines correspond to calculated curves based on Eqs. (3) and (4) with $D=8.3$ MHz. The transitions of Cr^{3+} are represented as: triangles, axial symmetry along [001]; squares, along [010], and circles, [100].

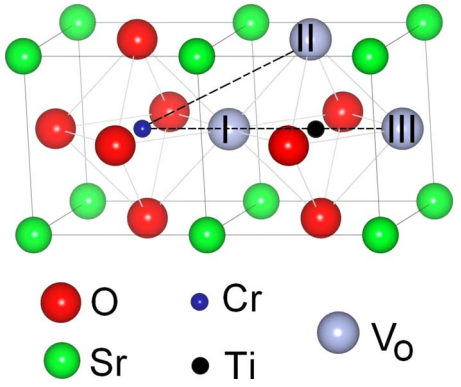

FIG. 9. (Color online) Crystal structure of Cr-doped $SrTiO_3$, showing the possible V_o position in the first three coordination spheres I, II, and III.

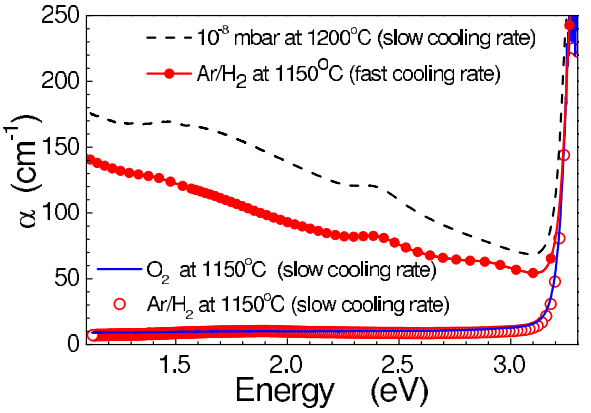

FIG. 10. (Color online) Optical absorption spectra of nominally pure $SrTiO_3$ annealed in different atmospheres.

eters, D and w. The analysis was performed for each spectrum in Fig. 6, yielding an average value $\bar{D}=8.3(8)$ MHz, corresponding to $\Delta\bar{B}_0=3.0(3)$ G. Figure 8 shows the peak position of the six lines as function of θ, and the continuous line is obtained by using $\bar{D}$.

At much lower Cr content, the value of D can be estimated directly from the spectra. In Fig. 5, three peaks are clearly distinguishable in the anisotropic component (dashed line). The maximum peak-to-peak distance corresponds to $4\Delta B_0$ in our fitting model, from which we estimate $D \simeq 7$ MHz ($\Delta B_0 \simeq 2.5$ G). This value is much smaller than the one found in Cr-doped WO_3,[44] where a V_o located next to the Cr site produces a much stronger axial field, $D \simeq 85$ GHz. Owing to the strong valence-bond character of the oxygen octahedron, a similar crystal-field splitting should be observed in $SrTiO_3$ for of a V_o directly attached to the Cr site (position I in Fig. 9). This discrepancy suggests that the V_o is located at the third coordination sphere along the ⟨100⟩ directions (position III in Fig. 9). A V_o in the second coordination sphere (position II in Fig. 9) is excluded because this geometry leads to a symmetry that is inconsistent with our result of an axial symmetry along ⟨100⟩.

C. Electron localization: Suppression of the conducting state

OA spectra taken at room temperature enable a comparison between conducting and insulating $SrTiO_3$ (Refs. 1 and 10) (Fig. 10). The undoped oxidized sample is insulating and transparent in the near-infrared and visible range with an absorption edge at 3.2 eV, corresponding to the an indirect band-gap transition of $SrTiO_3$.[30,45,46] The highly reduced sample, annealed in vacuum, exhibits absorption below the band gap, which can be assigned to the presence of V_os and conducting electrons.[1,47] However, the nominal pure $SrTiO_3$ crystals annealed in Ar/H_2 or O_2 (ambient pressure, at 1150 °C for 6 h), show identical OA spectra. These two particular thermal treatments were performed with a relatively slow cooling rate (≃−200 °C/h) from 1150 °C to room temperature. The comparison of the spectra in Fig. 10 suggest that the Ar/H_2 annealing is not able to significantly change the conducting properties of pure $SrTiO_3$. However, if the sample is quenched (in ≤60 sec) from 1150 °C to room temperature, the crystal became conducting and exhibits a similar OA spectrum as the pure $SrTiO_3$ annealed in high vacuum, as shown in Fig. 10. This means that at 1150 °C a significant amount of V_o is introduced because of the reducing atmosphere of Ar/H_2, but the cooling process can produce different effects: the slow cooling rate (≃−200 °C/h) assists the reoxidation of the crystal due to presence of a residual partial pressure of O_2; the fast cooling (quenching) freezes V_o in the crystal. A different behavior was observed in the case of Cr-doped crystals. The Ar/H_2 annealing causes the valence change in Cr from the 4+ to the 3+ state. Since Cr^{4+} ions are deep traps for CB electrons, at high temperature they capture electrons introduced by the V_o, and when the temperature is reduced slowly, the crystal is forced to keep an amount of V_o to compensate the charge trapped at the Cr^{3+} ions. In the doping range investigated, i.e., up to 2 mol %, all Cr atoms convert to the 3+ valence state, as demonstrated by the linear dependence of the EPR intensities of Cr^{3+} versus the Cr concentration shown in Fig. 11. At a content ≤0.01 mol%, the average distance between the Cr centers is ≥10 unit cells. Therefore, at this distance, an interaction between the Cr sites is expected to be negligible. As at all concentrations the Cr^{3+} centers exhibit the

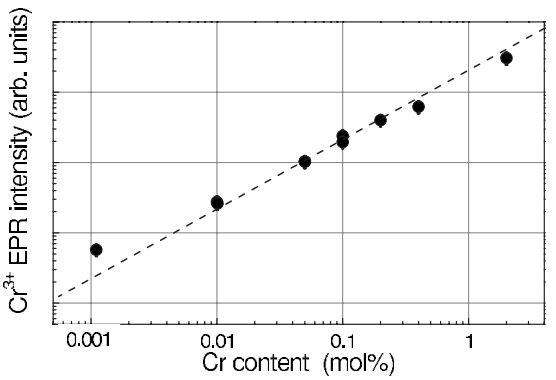

FIG. 11. Intensity of the EPR Cr^{3+} signal versus Cr content in reduced $SrTiO_3$. The linear dependence and the absence saturation at high doping show that all Cr ions are converted to the 3+ valence state.

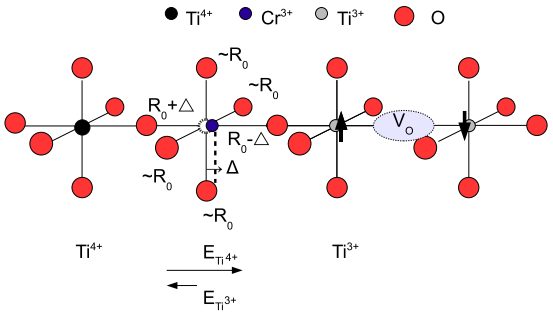

FIG. 12. (Color online) Model of the Cr^{3+}-O-Ti^{3+}-V_o-Ti^{3+} complex in reduced Cr-doped $SrTiO_3$ with the Cr^{3+} ion displaced by the distance Δ from the original 4+ position. The electric field generated by the two adjacent Ti^{3+} and Ti^{4+}, maybe responsible of the displacement Δ.

same axial symmetry, there must be a V_o perturbing each of the Cr sites. The absence of a saturation in the linear behavior suggests that the compensation arises from the effect of the thermal annealing on the Cr dopants and not from other impurities. Moreover, the linear behavior indicates that the charge compensation mechanism is the same at every doping level.

In the following, we discuss the possible mechanisms that change the valence of the Cr ions to the 3+ state and the origin of the Cr^{3+} axial symmetry. The electron captured by the Cr ion could come from the same V_o located at the third coordination sphere of the ion. In this case an unpaired electron should remain at the V_o center or a Ti^{4+} should be converted to Ti^{3+}. In both cases the magnetic dipolar interaction of these centers with the Cr^{3+} ion could give rise to an axial symmetry. According to Fig. 9, this electron should have an average distance from the Cr^{3+} ion on the order of $R_D=3\times R_0$, where R_0 is the distance between the Cr ion and the oxygen atom at the first coordination sphere. The magnitude of the field produced by this unpaired electron at the Cr^{3+} site is given by the expression[41]

$$B \simeq \frac{g\beta}{R_D^3} \simeq 93 \text{ G}. \tag{5}$$

This value is one order of magnitude larger than our experimental value observed as the splitting $\Delta B_0 \sim 3$ G. This discrepancy is consistent with the fact that we did not observe any other paramagnetic center except that of the Cr^{3+}. We have to conclude that, if an unpaired electron is present at the V_o site (or in form of Ti^{3+}) there must be a strong phonon coupling which masks this paramagnetic center via a strong spin-phonon relaxation. Another possible explanation is that there are two kinds of V_o centers introduced by the Ar/H_2 annealing: double charged vacancies (V_o^{++}) which could be randomly distributed and compensate the charges of the electrons trapped by the Cr ions and neutral V_os which are located at the third coordination sphere of the Cr^{3+} ions. In the case of the neutral V_o center, the two electrons from the missing bond of the nearest Ti ions are localized at the two adjacent Ti^{3+} with antiparallel spins[22] as shown in Fig. 12. This particular spin configuration is EPR silent.[48] Both kinds of oxygen vacancies are consistent with the model of strongly localized two-electron and two-hole excitation proposed by Anderson.[49]

The proximity of the Ti^{3+}-V_o-Ti^{3+} complex may be responsible of the breaking of the symmetry of the crystal field experienced by the Cr ion. As shown in Fig. 12, the Ti^{4+} repels the Cr^{3+} more than the nearest Ti^{3+}. The result of this Coulomb interaction produces a net attractive force on the Cr^{3+} toward the Ti^{3+}-V_o-Ti^{3+} complex. As a consequence, the Cr ion may result displaced from the center of the octahedron. Because of the strong covalent bond of the oxygen octahedron, we assume the displacement of the Cr ions as predominant reason of the axial symmetry. We now estimate the displacement of the Cr ion using the experimental value of the axial parameter D. For spin centers $S<2$, Newman and Urban[50] have shown that D can be expressed as a simple sum over the contribution of the separate coordinated ligands (denoted n):

$$D = \bar{b}_2(R_0)\left(\frac{3}{2}\right)\sum_1^6 \left(\frac{R_0}{R_n}\right)^{t_2}\left(\cos^2\Theta_n - \frac{1}{3}\right). \tag{6}$$

Here R_0 is distance between the Cr ion and the oxygen in an unperturbed octahedral site (Fig. 12), R_n is the distance between the Cr ion and the nth oxygen ligand in the distorted site, Θ_n is the angle between the line joining the paramagnetic ion with the nth ligand and main EPR axis, and $\bar{b}_2(R_0)$ and t_2 are coefficients that depend on R_0 and the nature of the ligand. These two coefficients have been evaluated by Müller and Berlinger[36] for Cr^{3+} on a metal 4+ site in $SrTiO_3$. In particular they replace the term $\bar{b}_2(R_0)\times(\frac{R_0}{R})^{t_2}$ in Eq. (6) with the function $\bar{b}_2(R)$, which can be approximated to a Lennard-Jones-type function described as:[36]

$$\bar{b}_2(R) = -A\left(\frac{R_0}{R}\right)^n + B\left(\frac{R_0}{R}\right)^m, \tag{7}$$

where $R_0=1.95$ Å, $A=-9.7(1.3)$ cm^{-1}, $B=-7.4(1.2)$ cm^{-1}, and the two exponents $m=10$ and $n=13$. From Eqs. (6) and (7) and the experimental D value, we calculated the displacement Δ (Fig. 12) of the Cr^{3+} as

$$D = \bar{b}_2(R_0+\Delta) + \bar{b}_2(R_0-\Delta) - 2\bar{b}_2(R_0). \tag{8}$$

We obtain $\Delta=0.06(2)$ Å, which corresponds to a displacement of only 3%. This result is in excellent agreement with a previous study of the EPR signal of Cr^{3+} in $SrTiO_3$ under a static uniaxial stress reported by Müller and Berlinger.[36] They found a value of $\Delta B_0 \simeq 2.8$ G, extrapolated at zero stress, which compares with our results of $\simeq 3$ G. They suggest that this axial symmetry may be explained in terms of a displacement of the Cr ion out of the center of the octahedral site along one of the ⟨100⟩ directions. Here we demonstrate that the axial symmetry is not an intrinsic property of the Cr^{3+}, but is a consequence of the nature of the charge compensation which generates the Cr^{3+} sites caused by the V_os. In the Cr/Nb-codoped crystal, with only Nb as a donor the Cr^{3+} remains in the center of a cubic site, whereas in the case of V_o compensation it shifts from the center. Other complexes of TM ions and V_os where the oxygen vacancy is

located in the first coordination sphere have been found in $SrTiO_3$, for example Fe^{3+}-V_o,[51] Mn^{2+}-V_o,[52] and Ni^{3+}-V_o,[48] However, the Cr^{3+}-V_o complex has never been observed with the V_o at the first coordination sphere. This fact may be explained in terms of the interaction between the Cr ion and the V_o. Once the Cr^{4+} traps an electron and becomes Cr^{3+}, the Coulomb interaction with the Ti^{3+} minimizes the energy to form the structure presented in Fig. 12. This particular complex could be the reason why all the reduced Cr-doped $SrTiO_3$ crystals we studied were insulating.

IV. CONCLUSIONS

Our EPR study of Cr-doped $SrTiO_3$ single crystals reveals changes in the symmetry of the Cr site that we control by means of thermal annealing and/or doping with electron donors. When electron donors are present, a Cr atom can change its valence from 4+ to 3+. If the Cr content is equal to or higher than that of the electron donors, the insulating state will be preserved. In a Cr/Nb-codoped crystal, we found that Cr^{3+} occupies an undistorted octahedral site, whereas in the Cr-doped reduced crystals there is a symmetry change from cubic to axial of the crystal field felt by the Cr atom. Here the full amount of Cr is converted to the 3+ state via a charge compensation involving V_os. For the Cr^{3+} in this complex, we found an axial crystal-field parameter $\bar{D}=8.3(8)$ MHz. Here we demonstrate that the axial symmetry observed at the Cr^{3+} site originates from the special location of a V_o which breaks the octahedral symmetry. The corresponding value of D is much lower than that of $\sim$42 GHz for Fe-V_o in $SrTiO_3$,[52] and $\sim$85 GHz for Cr-V_o in WO_3.[44] In these cases the axial symmetry has been assigned to V_os located in the first coordination sphere of the Fe or Cr sites. Our results on reduced crystals indicate, however, that the V_os in Cr-doped $SrTiO_3$ are located at the third coordination sphere. The charge neutrality of the sample and the axial symmetry of the Cr^{3+} can be explained with the presence of two kinds of oxygen vacancies: the neutral V_os and the double charged V_o^{++}s. The amount of both kinds of vacancies is directly controlled by the Cr concentration, and this correlation accounts for the preservation of the insulating state of the reduced Cr-doped crystals.

ACKNOWLEDGMENTS

We thank F. Waldner for providing his expertise for the EPR data analysis and for a careful reading of the manuscript. We thank Y. Watanabe and A. Maisuradze for fruitful discussions and valuable suggestions. F.L.M. gratefully acknowledges support by the Swiss National Science Foundation and the IBM Zurich Research Laboratory. We also thank D. Widmer, H. P. Ott, and K. Wasser for competent technical assistance.

[1] W. S. Baer, Phys. Rev. **144**, 734 (1966).
[2] O. N. Tufte and P. W. Chapman, Phys. Rev. **155**, 796 (1967).
[3] J. F. Schooley, W. R. Hosler, and M. L. Cohen, Phys. Rev. Lett. **12**, 474 (1964).
[4] C. S. Koonce, M. L. Cohen, J. F. Schooley, W. R. Hosler, and E. R. Pfeiffer, Phys. Rev. **163**, 380 (1967).
[5] G. Binnig, A. Baratoff, H. E. Hoenig, and J. G. Bednorz, Phys. Rev. Lett. **45**, 1352 (1980).
[6] C. H. Ahn, J. M. Triscone, and J. Mannhart, Nature (London) **424**, 1015 (2003).
[7] Y. Watanabe, Ferroelectrics **349**, 190 (2007).
[8] S. F. Alvarado, F. La Mattina, and J. G. Bednorz, Appl. Phys. A: Mater. Sci. Process. **89**, 85 (2007).
[9] F. La Mattina, J. G. Bednorz, S. F. Alvarado, A. Shengelaya, and H. Keller, Appl. Phys. Lett. **93**, 022102 (2008).
[10] A. Beck, J. G. Bednorz, C. Gerber, C. Rossel, and D. Widmer, Appl. Phys. Lett. **77**, 139 (2000).
[11] Y. Watanabe, J. G. Bednorz, A. Bietsch, C. Gerber, D. Widmer, A. Beck, and S. J. Wind, Appl. Phys. Lett. **78**, 3738 (2001).
[12] C. Rossel, G. I. Meijer, D. Bremaud, and D. Widmer, J. Appl. Phys. **90**, 2892 (2001).
[13] M. Janousch, G. I. Meijer, U. Staub, B. Delley, S. F. Karg, and B. P. Andreasson, Adv. Mater. **19**, 2232 (2007).
[14] M. J. Rozenberg, I. H. Inoue, and M. J. Sánchez, Phys. Rev. Lett. **92**, 178302 (2004).
[15] K. Szot, W. Speier, R. Carius, U. Zastrow, and W. Beyer, Phys. Rev. Lett. **88**, 075508 (2002).
[16] S. Karg, G. I. Meijer, D. Widmer, and J. G. Bednorz, Appl. Phys. Lett. **89**, 072106 (2006).
[17] K. Szot, W. Speier, G. Bihlmeyer, and R. Waser, Nat. Mater. **5**, 312 (2006).
[18] D. A. Müller, N. Nakagawa, A. Ohtomo, J. L. Grazul, and H. Y. Hwang, Nature (London) **430**, 657 (2004).
[19] D. Choi, D. Lee, H. Sim, M. Chang, and H. Hwang, Appl. Phys. Lett. **88**, 082904 (2006).
[20] Y. Watanabe, D. Sawamura, and M. Okano, Appl. Phys. Lett. **72**, 2415 (1998).
[21] L. Pellegrino, I. Pallecchi, D. Marre, E. Bellingeri, and A. S. Siri, Appl. Phys. Lett. **81**, 3849 (2002).
[22] D. Ricci, G. Bano, G. Pacchioni, and F. Illas, Phys. Rev. B **68**, 224105 (2003).
[23] N. Shanthi and D. D. Sarma, Phys. Rev. B **57**, 2153 (1998).
[24] J. Carrasco, F. Illas, N. Lopez, E. A. Kotomin, Y. F. Zhukovskii, R. A. Evarestov, Y. A. Mastrikov, S. Piskunov, and J. Maier, Phys. Rev. B **73**, 064106 (2006).
[25] D. D. Cuong, B. Lee, K. M. Choi, H.-S. Ahn, S. Han, and J. Lee, Phys. Rev. Lett. **98**, 115503 (2007).
[26] F. Cordero, Phys. Rev. B **76**, 172106 (2007).
[27] G. I. Meijer, U. Staub, M. Janousch, S. L. Johnson, B. Delley, and T. Neisius, Phys. Rev. B **72**, 155102 (2005).
[28] S. A. Basun, U. Bianchi, V. E. Bursian, A. A. Kaplyanskii, W. Kleemann, L. S. Sochava, and V. S. Vikhnin, Ferroelectrics **183**, 255 (1996).
[29] M. Capizzi and A. Frova, Phys. Rev. Lett. **25**, 1298 (1970).
[30] K. van Benthem, C. Elsässer, and R. H. French, J. Appl. Phys. **90**, 6156 (2001).

[31] S. A. Basun, U. Bianchi, V. E. Bursian, A. A. Kaplyanskii, W. Kleemann, L. S. Sochava, and V. S. Vikhnin, J. Lumin. **66-67**, 526 (1995).
[32] T. Feng, Phys. Rev. B **25**, 627 (1982).
[33] R. H. Hoskins and B. H. Soffer, Phys. Rev. **133**, A490 (1964).
[34] D. E. Budil, D. G. Park, J. M. Burlitch, R. F. Geray, R. Dieckmann, and J. Freed, J. Chem. Phys. **101**, 3538 (1994).
[35] K. A. Müller, Arch. Sci. **11**, 150 (1958).
[36] K. A. Müller and W. Berlinger, J. Phys. C **16**, 6861 (1983).
[37] H. D. Meierling, Phys. Status Solidi B **43**, 191 (1971).
[38] S. E. Stokowski and A. L. Schawlow, Phys. Rev. **178**, 457 (1969).
[39] J. J. Kawanabe, H. Minami, K. Oka, R. Oishim, and H. Uwe, Ferroelectrics **348**, 89 (2007).
[40] J. G. Bednorz and H. J. Scheel, J. Cryst. Growth **41**, 5 (1977).
[41] J. E. Wertz, *Electron Spin Resonance, Elementary Theory and Practical Applications* (Chapman and Hall, London, 1986).
[42] B. Bleaney, Physica **17**, 175 (1951).
[43] B. Bleaney and D. J. E. Ingram, Proc. R. Soc. London, Ser. A **205**, 336 (1951).
[44] T. Hirose and M. Kawaminami, J. Phys. Soc. Jpn. **50**, 843 (1981).
[45] S. I. Shablaev, A. M. Danishevskii, V. K. Subashiev, and A. A. Babashkin, Sov. Phys. Solid State **21**, 662 (1979).
[46] S. I. Shablaev, A. M. Danishevskii, and V. K. Subashiev, Sov. Phys. JETP **59**, 1256 (1984).
[47] C. Lee, J. Destry, and J. L. Brebner, Phys. Rev. B **11**, 2299 (1975).
[48] K. A. Müller, W. Berlinger, and R. S. Rubins, Phys. Rev. **186**, 361 (1969).
[49] P. W. Anderson, Phys. Rev. Lett. **34**, 953 (1975).
[50] D. J. Newman and W. Urban, Adv. Phys. **24**, 793 (1975).
[51] K. A. Blazey, J. A. Cabrera, and K. A. Müller, Solid State Commun. **45**, 903 (1983).
[52] E. S. Kirkpatrick, K. A. Müller, and R. S. Rubins, Phys. Rev. **135**, A86 (1964).